Bioorganometallic Chemistry. 13. Regioselective Reduction of NAD^+ Models, 1-Benzylnicotinamde Triflate and β-Nicotinamide Ribose-5′-methyl Phosphate, with in Situ Generated $[Cp^*Rh(Bpy)H]^+$: Structure−Activity Relationships, Kinetics, and Mechanistic Aspects in the Formation of the 1,4-NADH Derivatives†

H. Christine Lo,‡ Carmen Leiva,‡ Olivier Buriez,‡ John B. Kerr,‡ Marilyn M. Olmstead,§ and Richard H. Fish*,‡

Lawrence Berkeley National Laboratory, 70-108B, University of California, Berkeley, California 94720, and Department of Chemistry, University of California, Davis, California 95616

Received May 29, 2001

Cofactor regeneration; i.e., regiospecific conversion of NAD^+ to 1,4-NADH, has been extensively studied and is a crucial component in the eventual use of 1,4-NADH in a variety of bioorganic synthesis processes involving the formation of chiral organic compounds. We have studied the reduction of a model NAD^+ compound, 1-benzylnicotinamide triflate, **1a**, using $[Cp^*Rh(bpy)(H_2O)]^{2+}$, **2** ($Cp^* = \eta^5$-C_5Me_5, bpy = 2,2′-bipyridyl), as the catalyst precursor and sodium formate (HCO_2Na) as the hydride source in 1:1 H_2O/THF and have found exclusive 1-benzyl-1,4-dihydronicotinamide regioselectivity, as was observed previously for natural NAD^+ that provided 1,4-NADH (see: Steckhan et al. *Organometallics* **1991**, *10*, 1568). Moreover, a variety of 3-substituted derivatives of 1-benzylpyridinium triflate, in addition to the $-C(O)NH_2$ group (**1a**), were also studied to ascertain that this 3-functionality (e.g., $-C(O)NHCH_3$, $-C(S)NH_2$, $-C(O)CH_3$, $-C(O)OCH_3$, and $-CN$, **1b,d−g**) coordinates to a $[Cp^*Rh(bpy)H]^+$ complex to direct the concerted, regioselective transfer of the hydride group from the rhodium to the 4-ring position of the NAD^+ model; all coordinating 3-substituents had relative rates in the 0.9−1.3 range with substrate **1a** set to 1.0. If in fact the 3-substituent presented a steric effect [$-C(O)NH(CH_2CH_3)_2$, **1c**] or was a nonbinding group ($-CH_3$, **1h**; $-H$, **1i**), no catalytic hydride transfer was observed even with the more electrophilic 2 and 6 ring positions being readily available, which further implicated the crucial coordination of the NAD^+ model to the Cp*Rh metal ion center. We also found that the 1-benzyl substituent on the nitrogen atom exerted a substantial electron-withdrawing effect, in comparison to the electron-donating 1-methyl substituent, and favorably affected the rate of the regioselective reduction (rate enhancement of 1-benzyl/1-methyl = 2.0). The kinetics of the regioselective reduction of **1a** were studied to show that the initial rate of reduction, r_i, is affected by the concentrations of the substrate, **1a**, precatalyst, **2**, and the hydride source, HCO_2Na, in 1:1 H_2O/THF: d[1-benzyl-1,4-dihydronicotnamide]/dt = k_{cat}[**1a**][**2**][HCO_2Na]. Furthermore, we wish to demonstrate that a previously synthesized aqueous NAD^+ model, β-nicotinamide ribose-5′-methyl phosphate, **3**, shows a similar regioselectivity for the 1,4-NADH analogue, while the initial rate (r_i) for the regioselective reduction of **3** and NAD^+ itself was found to be comparable in water but faster by a factor of ∼3 in comparison to **1a** in 1:1 H_2O/THF; the solvent, THF, appeared to inhibit the rate of reduction in **1a** by presumably competing with the substrate **1a** for the Cp*Rh metal ion center. However, in H_2O, the initial kinetic rate for substrate **3** was not affected by its concentration and implies that, in H_2O, $[Cp^*Rh(bpy)H]^+$ formation is rate determining. We assume that binding of **3** and NAD^+ to the Cp*Rh metal ion center is also a pertinent step for 1,4-dihydro product formation, the experimental rate expression in H_2O being d[1,4-dihydro-β-nicotinamide ribose-5′-methyl phosphate]/dt = k_{cat}[**2**][HCO_2Na]. What we have discovered, for the first time, is evidence that the regioselective reduction of NAD^+ to 1,4-NADH by $[Cp^*Rh(bpy)H]^+$ is a consequence of the amide's ability to coordinate to the Cp*Rh metal center, thereby constricting the kinetically favorable six-membered ring transition state for plausible concerted hydride transfer/insertion to C4 to regioselectively provide the 1,4-NADH derivative; $[Cp^*Rh(bpy)H]^+$ can be categorized as a biomimetic enzymatic hydride via its ability to bind and regioselectively transfer hydride to C4, exclusively. Clearly, the pyrophosphate and adenosine groups associated with the structure of NAD^+ are not essential in the rate of hydride transfer to C4, with NAD^+ model **3** having a similar initial rate (r_i) of reduction as NAD^+ itself in water. Finally, a catalytic cycle will be proposed to account for our overall observations.

Introduction

Practical methods for the regeneration of the coenzyme 1,4-NADH, the reduced form of nicotinamide adenine dinucleotide (NAD^+), have continued to be of significant importance in the biocatalysis field, where enzymatic reduction reactions are critical for chiral, organic compound synthesis.[1a,b] Conversion of NAD^+ to 1,4-NADH by enzymatic, chemical, photochemical, or electrochemical methods has been extensively studied to increase the rate of the regeneration, while maintaining the

* Corresponding author. Phone: 510-486-4850. Fax: 510-486-7303. E-mail: rhfish@lbl.gov.

† Dedicated to the memory of Dr. E. Steckhan, whose pioneering studies in the reduction of NAD^+ with organometallic hydrides was an inspiration for our presented results.

‡ University of California at Berkeley.

§ University of California at Davis.

(1) (a) Chenault, H. K.; Whitesides, G. M. *Appl. Biochem. Biotechnol.* **1987**, *14*, 147. (b) Fang, J. M.; Lin, C. H.; Bradshaw, C. W.; Wong, C. H. *J. Chem. Soc., Perkin Trans 1* **1995**, 967.

10.1021/ic010562z CCC: $20.00
Published on Web 11/10/2001

necessary 1,4-dihydro regioselectivity. However, the cofactor regeneration is frequently the economic limiting factor in the eventual use of 1,4-NADH in enzymatic, chiral synthesis reactions, particularly for larger volumes and more energy intensive processes.[1,2]

To develop faster rates and a more economical regeneration process, various transition metal hydrides have been studied as catalysts for the regioselective reduction of NAD^+ and NAD^+ models to the 1,4-NADH derivatives.[2a−g] In the most illustrative example, Steckhan and co-workers have described the use of in situ generated $[Cp^*Rh(bpy)H]^+$ for the regiospecific reduction of NAD^+ to 1,4-NADH (eq 1)[2b] and then demonstrated the cofactor regeneration process in tandem with enzymatic, chiral reduction reactions.[3,4]

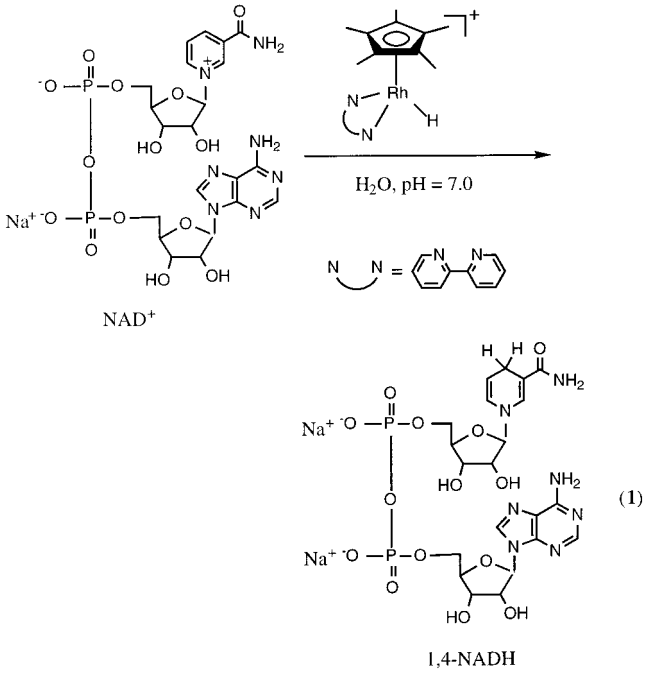

(1)

While the above-mentioned reduction of NAD^+ by $[Cp^*Rh(bpy)H]^+$ was shown,[2b,5a] at that time, to be highly regiospecific for 1,4-NADH, the mechanistic details of this important cofactor conversion and the role of the substituents on the nicotinamide moiety (3-amide and 1-ribose groups) were only recently elucidated by our group in a preliminary communication.[6] Thus, we reported on the source of this regioselectivity and other mechanistic aspects with a model NAD^+ compound, 1-benzylnicotinamide triflate,[7] **1a**, using $[Cp^*Rh(bpy)(H_2O)](OTf)_2$, **2**, as the catalyst precursor and sodium formate as the hydride source in 1:1 H_2O/THF; THF was necessary to solubilize the 1-benzyl-1,4-nicotinamide product.[2b] Furthermore, we also reported on a variety of 3-substituted derivatives of 1-benzylpyridinium triflate (**1b**−**i**) to ascertain how other substituents in the 3-position would influence the regioselectivity (1:1 H_2O/THF). Additionally, we were also interested in examining any steric and electronic effects that these 3-substituents and, as well, the 1-substituent, might impart on the rate of hydride transfer.

In this account, we wish to present full details of our synthetic, kinetic, and mechanistic studies with a variety of 3-pyridinium NAD^+ models in 1:1 H_2O/THF and, furthermore, to introduce an aqueous NAD^+ model, β-nicotinamide ribose-5′-methyl phosphate, **3**, which allows further comparison, both structurally and for the fact that the 1,4-dihydro derivative of **3** was water soluble, to NAD^+ itself in the kinetics and mechanisms of the regioselective reduction reaction. We will also present a plausible catalytic cycle that accommodates our extensive experimental results.

Results

Synthesis of NAD^+ Models, 1a−i. The pyridinium NAD^+ models, with a variety of 3-substituents, were synthesized according to the following method in high yields (eq 2).[7a,b] These 3-substituents were utilized to provide crucial information on binding, steric, and electronic effects in their regioselective reductions conducted in 1:1 H_2O/THF.

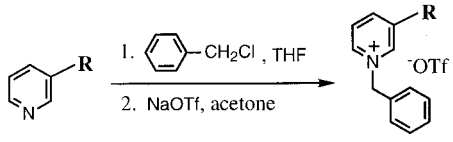

(2)

R = -C(O)NH_2, **a**; -C(O)$NHCH_3$, **b**; -C(O)$N(C_2H_5)_2$, **c**; -C(S)NH_2, **d**; -C(O)CH_3, **e**; -C(O)OCH_3, **f**; -CN, **g**; -CH_3, **h**; -H, **i**.

***β*-Nicotinamide Ribose-5′-Methyl Phosphate: A New Aqueous NAD+ Model.** While the NAD^+ models **1a**−**i** afforded the basis for resolving the various binding, steric, and electronic effects, the synthesis of an aqueous NAD^+ model with structural characteristics more aligned with the natural NAD^+, i.e., ribose and phosphate groups, and its 1,4-dihydro derivative, 1,4-NADH, was important for our model cofactor regeneration studies to fully delineate the role, if any, of the NAD^+ pyrophosphate and adenosine moieties on the rate of the regioselective reduction. Therefore, we synthesized a previously reported, but poorly characterized, NAD^+ model, **3**,[7c] from a commercially available precursor, β-nicotinamide ribose-5′-phosphate, via a different methylation reaction using dicyclohexylcarbodiimide (DCC) and a catalytic amount of *p*-(dimethylamino)pyridine (DMAP) in methanol with an isolated yield of 52% (eq 3); the CPK model of **3** is also provided for conformational information.

X-ray Crystal Structure of $[Cp^*Rh(bpy)(H_2O)](OTf)_2$, 2. The reaction of $[Cp^*Rh(H_2O)_3](OTf)_2$ with 2,2′-bipyridine in water provided $[Cp^*Rh(bpy)(H_2O)](OTf)_2$, **2**, in 77% isolated yield. This complex, **2**, containing a noncoordinating OTf^- anion, was utilized as a precatalyst in the subsequent regiose-

(2) (a) Ruppert, R.; Herrmann, S.; Steckhan, E. *J. Chem. Soc., Chem. Commun.* **1988**, 1150. (b) Steckhan, E.; Herrmann, S.; Ruppert, R.; Dietz, E.; Frede, M.; Spika, E. *Organometallics* **1991**, *10*, 1568 and references therein. (c) Hembre, R. T.; McQueen, S. *J. Am. Chem. Soc.* **1994**, *116*, 2141. (d) Collman, J. P.; Wagenknecht, P. S.; Lewis, N. S. *J. Am. Chem. Soc.* **1992**, *114*, 5665 and references therein. (e) Collman, J. P. *Nat. Struct. Biol.* **1996**, *3*, 213 and references therein. (f) Beley, M.; Collin, J.-P. *J. Mol. Catal.* **1993**, *79*, 133. (g) Umeda, K.; Ikeda, H.; Nakamura, A.; Toda, F. *Chem. Lett.* **1992**, 353. (h) Umeda, K.; Nakamura, A.; Toda, F. *Bull. Chem. Soc. Jpn.* **1993**, *66* 2260 and references therein.

(3) Steckhan, E.; Herrmann, S.; Ruppert, R.; Thommes, J.; Wandrey, C. *Angew. Chem., Int. Ed. Engl.* **1990**, *29*, 388.

(4) (a) Ruppert, R.; Herrmann, S.; Steckhan, E. *Tetrahedron Lett.* **1987**, *28*, 6583. (b) Westerhausen, D.; Herrmann, S.; Hummel, W.; Steckhan, E. *Angew. Chem., Int. Ed. Engl.* **1992**, *31*, 1529.

(5) (a) An analogue of $[Cp^*Rh(bpy)H]^+$, $[Cp^*Rh(6,6′\text{-dimethyl-}2,2′\text{-bipy})H]^+$, was identified by ^1H NMR.[2b] (b) Pathways for the hydride decomposition were discussed; see: Kölle, U.; Kang, B.-S.; Infelta, P.; Compte, P.; Grätzel, M. *Chem. Ber.* **1989**, *122*, 1869.

(6) Lo, H. C.; Buriez, O.; Kerr, J. B.; Fish, R. H. *Angew. Chem., Int. Ed. Engl.* **1999**, *38*, 1429.

(7) (a) Mauzerall, D.; Westheimer, F. H. *J. Am. Chem. Soc.* **1955**, *77*, 2261. (b) Kimura, E.; Shionoya, M.; Hoshino, A.; Ikeda, T.; Yamada, Y. *J. Am. Chem. Soc.* **1992**, *114*, 10134. (c) Miller, M.; Czochralska, B.; Shugar, D. *Bioelectrochem. Bioenerg.* **1982**, *9*, 287.

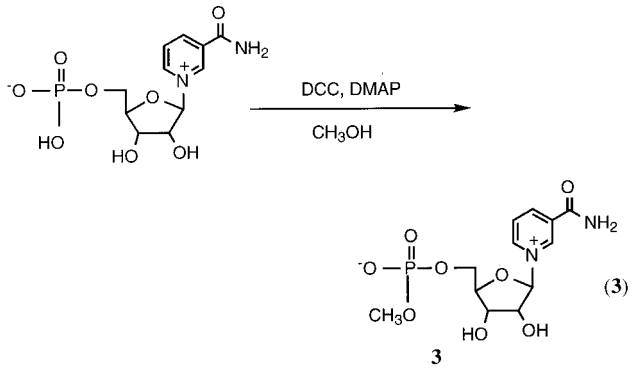

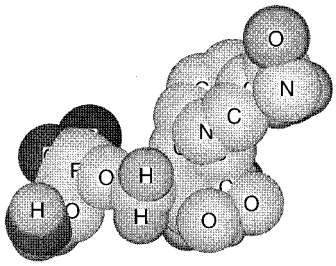

lective reduction reactions. More importantly, the structure of complex **2** was determined by single-crystal X-ray analysis, since the aqua complex had not been previously published, but was mentioned in a footnote as being disordered in the anion (Figure 1).[8] The crystallographic information and selected bond lengths and angles for the typical piano stool structure of **2** are given in Tables 1 and 2 (in text).

Regioselective Reductions of NAD$^+$ Models by Using Sodium Formate as Hydride Source and [Cp*Rh(bpy)(H$_2$O)](OTf)$_2$, 2, as the Precatalyst. The initial experiments to define the mechanism of the regioselective reduction reaction, as depicted in eq 1, were conducted utilizing ^{1}H NMR spectroscopy in 1:1 D$_2$O/THF-d_8 with NAD$^+$ model **1a** and precatalyst **2** in the presence of the hydride source, HCO$_2$Na, that showed that both 1-benzyl-1,4-dihydronicotinamide, **4a** (>95%), and its 1,6-isomer (<5%) were formed (eq 4); to reiterate, THF was used as a cosolvent, since **4a** was not totally soluble in H$_2$O at the concentrations utilized for the NMR experiments.

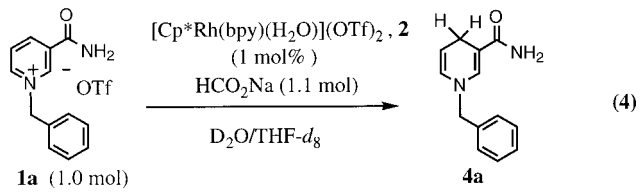

However, the 1,4-dihydro product, **4a**, was separately found to be converted, under similar reaction conditions, to <5% (2 h) of the 1,6-dihydro isomer via a complex **2** catalyzed rearrangement (eq 5) to fully account for the presence of this minor product in eq 4. Thus, as with NAD$^+$, model **1a** also

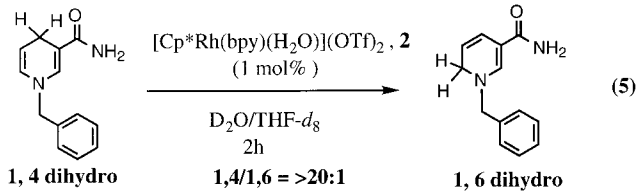

provides high regioselectivity for the 1,4-dihydro product with

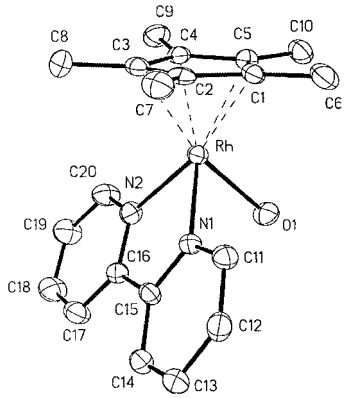

Figure 1. X-ray structure of the complex [Cp*Rh(bpy)(H$_2$O)](OTf)$_2$, **2**.

Table 1. Crystallographic Data for Complex **2**

compd	[Cp*Rh(bpy)(H$_2$O)]OTf$_2$
formula	$C_{22}H_{25}F_6N_2O_7RhS_2$
cryst size	0.40 × 0.36 × 0.16 mm
cryst habit	parallelepiped
cryst color	yellow
cryst system	monoclinic
space group	$P2_1/c$
unit cell dimens	a =12.411(3) Å, α = 90°
	b = 15.811(3) Å, β = 97.44(3)°
	c = 14.258(3) Å, γ = 90°
V	2774.3(10) Å^3
Z	4
D_{calc}	1.741 g cm^{-1}
abs coeff	0.854 mm^{-1}
abs corr	XABS2
F_{000}	1470
temp	130(2) K
wavelength	0.710 73 Å (Mo Kα)
θ range for data collection	1.65−27.59°
goodness-of-fit on F^2	1.042
reflcns collcd	8986
indpdt reflcns	6371 (R_{int} = 0.0520)
obsd data (>2σ(I))	4701
R indices calcd from obsd data	R1 = 5.35%, wR2 = 10.1%

Table 2. Selected Bond Lengths (Å) and Bond Angles (deg) for **2**

Bond Lengths			
Rh−N(1)	2.093(4)	Rh−N(2)	2.115(4)
Rh−C(1)	2.151(4)	Rh−C(2)	2.161(4)
Rh−C(3)	2.141(4)	Rh−C(4)	2.182(4)
Rh−C(5)	2.174(4)	Rh−O(1)	2.157(3)
Bond Angles			
N(1)−Rh−N(2)	77.50(14)	N(1)−Rh−C(1)	109.1(2)
N(2)−Rh−C(1)	167.2(2)	N(1)−Rh−C(2)	97.3(2)
C(1)−Rh−O(1)	109.2(2)	O(1)−Rh−C(2)	146.4(2)

[Cp*Rh(bpy)H]$^+$ but is mitigated, as was also found for NAD$^+$ itself in similar experiments, to a very minor extent (<5%), via a complex **2** catalyzed rearrangement of the kinetic product, **4a**, to the 1,6-dihydro isomer; the overall ratio of **4a** to its 1,6-isomer was found to be >20:1 in eq 4, while the origin of the 1,6-dihydro isomer was verified in eq 5. More importantly, when we used DCO$_2$Na (98% D) as the hydride source, the deuterium was found to be incorporated almost *exclusively* at the C$_4$ position (>95%, ^{1}H NMR shows a broad singlet at δ 3.28 for two H4 protons for **4a** and remains a broad singlet integrating for one proton upon addition of one D to **1a**, while the diagnostic H5 proton becomes a simple doublet from a doublet of triplets at δ 4.94) rather than the C$_6$ position (ratio of H6 to H4 is now

(8) Kölle, U.; Grätzel, M. *Angew. Chem., Int. Ed. Engl.* **1987**, *26*, 567.

Table 3. Relative Rates and Turnover Frequencies of the Regioselective Reductions of NAD^+ Models[a]

substrate	R	relative rate[b]	turnover/h[c]
1a	$C(O)NH_2$	1.0	9
1b	$C(O)NHCH_3$	0.9	8
1c	$C(O)NEt_2$	0.0	0
1d	$C(S)NH_2$	1.3	11
1e	$C(O)CH_3$	1.0	9
1f	$C(O)OCH_3$	1.3	11
1g	- CN	0.9	8
1h	- CH_3	0.0	0
1i	- H	0.0	0

[a] See eq 5. The reactions were conducted in presilylated J. Young NMR tubes and were followed by ^1H NMR. [b] The relative rates were determined by observing the disappearance of the pyridinium signals versus an internal standard, $[(CH_3)_4N]OTf$, during the first 2 h, where the relative rate of **1a** was set to 1.0. [c] The turnover frequencies were calculated by the mmol of product/mmol of catalyst/h. The total turnover number in 24 h is ~95 for all substrates that give product.

~1:1 (± 5% error) in **4a** with one deuterium at C4), therefore, further defining the initial kinetic product as being the 1,4-isomer, **4a**.

Furthermore, it was noted that deuteration of H4 in both **1a** and **4a** was observed in the ^1H NMR spectrum of the reaction mixture in 1:1 D_2O/THF, after a prolonged reaction time (>24 h). For example, the **1a** signal for H4 (δ 8.81, d) was found to disappear, while the two H4 protons in **4a** (δ 3.28, br s) were also completely deuterated as shown in the ^1H NMR spectrum of the reaction mixture (>24 h). A control experiment clearly showed that H4 deuteration of **1a** was not detected in the presence of the precatalyst **2** in D_2O, and thus, the observed deuteration of the H4 proton in **1a**, **1a**-*d*, appears to emanate from $[Cp^*Rh(bpy)D]^+$, formed possibly via exchange of $[Cp^*Rh(bpy)H]^+$ with D_2O.[9] These latter deuterium exchange results, while complicated, imply that overall reversibility for the regioselective reduction might be a possibility, although at very slow rates.

Table 3 demonstrates the relative rates (**1a**, set to 1.0) and turnover frequencies (TOF) for the other 3-substituted 1-benzylpyridinium compounds, which also provide the regioselective 1,4-dihydro products under the same reaction conditions as shown in eq 4: $-C(O)NHCH_3$, **1b**; $-C(S)NH_2$, **1d**; $-C(O)CH_3$, **1e**; $-C(O)OCH_3$, **1f**; $-CN$, **1g** (eq 6). Additionally, the complex **2** catalyzed rearrangement of the 1,4-dihydro derivatives, **4b,d−g**, to the corresponding 1,6-dihydro derivative (as described in eq 5) was also observed, similar to **4a**, to be in the range of ~5−15%.

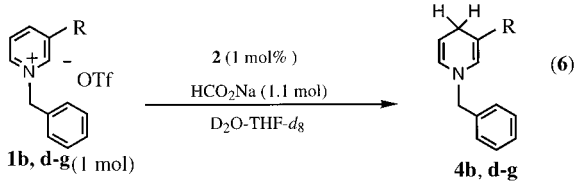

(6)

What is strikingly clear about the results in Table 3 is the total lack of 1,4-dihydro product formation with the noncoordinating, electron-donating $-CH_3$, **1h**, or the $-H$, **1i**, group; rather, we observe the apparent decomposition of the $[Cp^*Rh(bpy)H]^+$ complex, and this occurs rapidly with several broadened Cp*Rh signals being observed. Only the signals for **1h,i** were present, and no signal for **2** was evident.[5b] Moreover, attempts to define the formation of $[Cp^*Rh(bpy)H]^+$ via generation in the absence of substrate showed formation of CO_2 bubbles and a blue color after ~30 min, but no evidence of hydride signals in the −7 ppm range. Therefore, we conclude in the absence of a binding substrate, or no substrate, that $[Cp^*Rh(bpy)H]^+$ is extremely unstable under our reaction conditions.[5b] In contrast, replacement of a 3-substituent with potential coordinating ability, for example, the $-C(S)NH_2$ group in **1d**, increased the relative rate by ~30% in comparison to the $-C(O)NH_2$ group, **1a**, and this suggests that the more polarizable, soft S atom, a better σ-donor, coordinates readily to the Cp*Rh metal center and, thereby, facilitates hydride transfer to C4. Moreover, the 3-substituent, $-C(O)OCH_3$, in **1f**, also increased the relative rate by ~30%, in comparison to **1a**, presumably for reasons associated with its coordinating ability. If the potential coordinating substituent binds to the Cp*Rh, this also provides an electron-withdrawing effect that increases the electrophilicity of C4 and would also facilitate hydride transfer to that carbon atom.

Further convincing evidence for the critical coordination step, found to be apparently essential for the observed regioselectivity, came when the $-C(O)NH_2$ group ($E_p = -1.23$V vs Ag/AgCl) in **1a** was replaced with a $-C(O)NEt_2$ group ($E_p = -1.26$V vs Ag/AgCl), **1c**. We observed no detectable 1,4-dihydro product via ^1H NMR and only $[Cp^*Rh(bpy)H]^+$ decomposition, even though both substituents would be of equal σ-donating ability and overall electronic effect. A plausible explanation would entail that steric interactions between the Cp* methyl groups and the 3-substituent ethyl groups (NEt_2) inhibit coordination of substrate to the Cp*Rh metal center, thereby limiting the hydride transfer process. More interestingly, this result occurs even with the most electrophilic and sterically unencumbered C6 position of **1c** being readily available, strengthening the concept of plausible coordination of the carbonyl of the $-C(O)NH_2$ group, **1a**, to the Cp*Rh metal center, as well as those substituents in substrates **1b,d−g**.[10]

Comparing the σ-Donating Ability and the Electron-Withdrawing Substituent Effect via Competitive Regioselective Reduction Reactions: 1a versus 1e,g and 1a versus 1d,f. To further establish whether the σ-donating ability or the electron-withdrawing effect of the 3-substituent was the more important parameter, several competitive substrate reduction experiments were performed. We found that when we reduced **1a** in the presence of either **1e** ($E_p = -1.08$ V vs Ag/AgCl) or **1g** ($E_p = -0.97$ V vs Ag/AgCl) substrate **1a** with a $-C(O)NH_2$ group was slightly more reactive than either the $-C(O)CH_3$ or $-CN$ analogues (1.1 and 1.3 times faster, respectively), and if we reduced **1a** in the presence of **1d** or **1f**, the $-C(S)NH_2$ and $-C(O)OCH_3$ derivatives were both found to be more reactive (1.3 and 1.2 times faster, respectively). Thus,

(9) (a) *Transition Metal Hydrides*; Muetterties, E. L., Ed.; Marcel Dekker: New York, 1971. (b) For a recent study, see: Paterniti, D. P.; Roman, P. J., Jr.; Atwood, J. D. *Organometallics* **1997**, *16*, 3371 and references therein.

(10) The coordination of the $-CN$ substituent through the π-electrons as a 2e or 4e donor has been reported; see: Cotton, F. A.; Wilkinson, G. *Advanced Inorganic Chemistry*, 5th ed.; Wiley: New York, 1988; p 254 and references therein.

we tentatively conclude that the σ-donating ability of the 3-substituent (e.g. **1a,d,f**) is a slightly more important parameter (binding to Cp*Rh) than the incipient electron-withdrawing effect of this group (e.g. **1e,g**) in the overall reduction reaction. However, it is important to note that the two effects are balanced on one side by the better σ-donating ability and, thus, increase in hydride reactivity, while the electron-withdrawing substituent provides a more electrophilic C4 center but a weaker hydride transfer step. These balancing effects are consistent with the relative rates shown in Table 1, where all coordinating substituents have essentially similar values.

Electronic Effect of 1-Substituted Nicotinamide Substrates on the Relative Rate/Turnover Frequency of the Regioselective Reduction. We also examined the possible electronic effect of substituents bound to the nitrogen atom of the nicotinamide nucleus. Thus, we replaced the 1-benzyl group (**1a)** with a 1-methyl group, 1-methylnicotinamide, substrate **5** ($E_p = -1.31$ V vs Ag/AgCl), and found that this change in substituent reduced the relative rate to 0.5, providing a relative rate ratio of 1-benzyl/1-methyl of 2.0 (1:1 D_2O/THF; see Table 3 for experimental conditions). The implication of this latter result is that the 1-benzyl group is an electron-withdrawing substituent in comparison to the electron-donating 1-methyl group, and this further facilitates hydride attack at C4; plausible electron reorganization upon hydride transfer to C4 would benefit from a through bond electron-withdrawing substituent on the nitrogen atom of the nicotinamide nucleus.

The aqueous NAD^+ model, **3**, with ribose as the 1-substituent, was also compared to **1a** for turnover frequency (TOF, ^{1}H NMR data, D_2O, unbuffered) in the regioselective reduction (eq 7) and was found to provide 20 h^{-1} or ~2.5 times those for the TOF for **1a** (Table 3). It is important to note that natural NAD^+ had a similar TOF of 18 h^{-1} under the standard conditions, as shown in eq 7. The two factors that must be considered for this TOF increase include the electronic effect of the sugar as the 1-substituent (compared to the 1-benzyl group) and conceivably the solvent effects of THF and water; both factors, as of now, appear important for this substantial TOF increase.

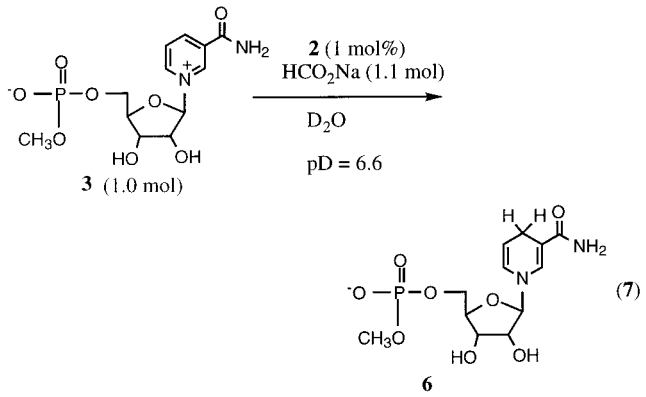

(7)

Kinetic and Activation Parameters for the Regioselective Reduction of NAD^+ Models, 1a and 3, with [Cp*Rh(bpy)H]$^+$: Comparison to NAD^+. The kinetics of the regioselective reduction reactions were further studied by utilizing UV−vis techniques with the two NAD^+ model substrates, **1a** and **3**, and the results compared to NAD^+ itself. We were able to ascertain the effect of the initial rate (r_i) at low conversions to the 1,4-dihydro product (~10%) by varying the substrates, precatalyst, **2**, and sodium formate concentrations. The initial rates, r_i, in 1:1 H_2O/THF, of the regioselective reduction (Supporting Information) were found to be concentration dependent in substrate **1a**, precatalyst [Cp*Rh(bpy)(H_2O)]-$(OTf)_2$, **2**, and sodium formate (the hydride source) from the plots of r_i (M s^{-1}) vs concentration of **1a**, precatalyst **2**, and HCO_2Na (M) (Figure 2).

Further verification of the reaction order of the **1a**, **2**, and HCO_2Na was determined from plots of ln r_i vs ln [**1a**], ln [**2**], and ln [HCO_2Na], which provided slopes of 1.1, 1.0, and 0.7, respectively (Supporting Information). Therefore, the experimental rate law as determined in 1:1 H_2O/THF is as follows (eq 8) with $k_{cat} = 2.25$ M^{-2} s^{-1} at 299.7 K:

$$d[\mathbf{4a}]/dt = k_{cat}[\mathbf{1a}][\mathbf{2}][HCO_2Na] \quad (8)$$

The influence of the solvent THF on the rate of formation of 1-benzyl-1,4-dihydronicotinamide, **4a** (Supporting Information), was also studied, since we observed an initial rate enhancement in water with substrates **3** and NAD^+ (Supporting Information) compared to **1a** in 1:1 H_2O/THF. It was observed that decreasing the concentration of THF and, therefore, changing the H_2O/THF ratio from 1:1 to 4:1 caused the initial rate of formation of the 1,4-dihydro derivative to increase by a factor of >6 at comparable concentrations.

This decrease in rate result suggested that THF was possibly in competition with **1a** for the catalyst, [Cp*Rh(bpy)H]$^+$, metal ion center and plausibly affected the substrate-catalyst binding step.[6] Another possibility for THF inhibition resides in the formation of the [Cp*Rh(bpy)(OC(O)H)]$^+$ intermediate via reaction of formate with precatalyst **2**;[2b] however, with the observation that the initial rate of reduction is dependent upon the concentration of [**1a**] tends to favor the substrate binding step being critical for product formation.[6] Further definitive proof of the importance of the substrate−catalyst binding step comes from the observation of no reduction of **1c** in comparison to **1a**, because of presumed steric demands that prevent **1c** from binding to the Cp*Rh metal ion center; i.e., if binding of substrate to catalyst was not crucial, then **1c** would have provided product with the further stipulation that the 6 ring position of **1c** is also readily available for hydride attack. It is also important to note that the initial rates of reduction of **1a** in 4:1 H_2O/THF (Supporting Information) are now comparable to **3** and NAD^+ in water, and plots of initial rate (r_i) versus concentration of **1a** still show some effect on rate, but the ln r_i vs ln concentration of **1a** plot provides a 0.5 order; decreasing from an order of 1.0 in 1:1 H_2O/THF.

The effect of concentration of substrate **3** in water at pH 6.5 on the rate of the regioselective reduction also provided a difference, in comparison to **1a** (1:1 H_2O/THF), in that there was no effect on rate, which implicates a zero-order dependence of **3** on the initial rate, consistent with the findings of Steckhan et al. for NAD^+.[2b] Therefore, the experimental rate law as determined in H_2O, is as follows (eq 9) with $k_{cat} = 3.98 \times 10^{-1}$ M^{-1} s^{-1} at 303 K:

$$d[\mathbf{6}]/dt = k_{cat}[\mathbf{2}][HCO_2Na] \quad (9)$$

The temperature effect on the rate constant, k_{cat}, was studied in the range of 282−303 K for NAD^+ model **1a** (1:1 H_2O/THF) at concentrations of 4.29×10^{-3} M, complex **2** at 4.33×10^{-5} M, and HCO_2Na at 0.0539 M, while the temperature effect was studied for **3** (H_2O) at concentrations of 1.48×10^{-3} M, complex **2** at 1.42×10^{-5} M, and HCO_2Na at 0.0186 M; results for NAD^+ were compared to those of model **3** (Supporting Information). An Arrhenius plot of ln k_{cat} versus $1/T$ allowed us to determine the activation energy, E_a, while the other activation parameters, such as the enthalpy, entropy, and

Table 4. Activation Parameters for Substrates **1a**, **3**, and NAD^+

	substrate		
	1a (1:1 H_2O−THF)	**3** (H_2O)[a]	NAD^+ (H_2O)
E_a (kcal/mol)	15.91 ± 0.68	25.26 ± 1.01	24.11 ± 0.42
$\Delta H^‡$ (kcal/mol)	15.34 ± 0.67	24.67 ± 1.00	23.53 ± 0.42
$\Delta S^‡$ (eu)	−5.97 ± 0.32	20.81 ± 1.42	16.78 ± 1.43
$\Delta G^‡$ (kcal/mol)[b]	17.12 ± 0.77	18.47 ± 1.42	18.53 ± 0.85

[a] H_2O, pH = 6.5. [b] At 298 K.

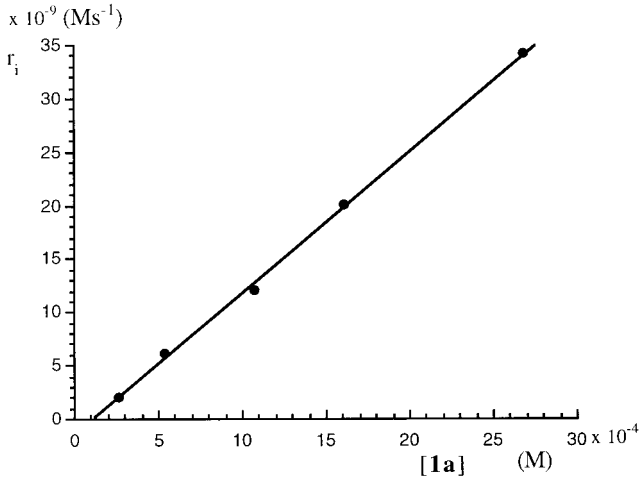

Figure 2. Plot of initial rate (r_i) versus [**1a**] concentration.

free energy of activation were obtained as follows: $\Delta H^‡$, $\Delta S^‡$ from Eyring plots of ln k_{cat}/T versus $1/T$; $\Delta G^‡ = \Delta H^‡ - T\Delta S^‡$ for model **1a**, **3**, and NAD^+ (Table 4 and Supporting Information).

Discussion

Mechanism of the Regioselective Reduction of NAD^+ Models. It was highly important to elucidate the mechanism of the regioselective reduction of natural NAD^+, via the use of the in situ generated $[Cp^*Rh(bpy)(H)]^+$, to fully clarify the unusual propensity for the biologically active 1,4-NADH analogue and to further define the role of each substituent on the NAD^+ nucleus, with emphasis on the 3-amide and 1-ribose groups, and, as well, if the pyrophosphate/adenosine constituents of NAD^+ affected the rates of reduction.[2] The initial ^1H NMR experiments with substrates **1a**−**i** in 1:1 H_2O/THF (Table 3) were very enlightening in that what was evident was the crucial ability of the 3-substituent to bind to the Cp*Rh metal center to obtain the corresponding 1,4-dihydro derivative; i.e., if a group had a pronounced steric effect (substrate **1c**) or was nonbinding in the 3-position (substrates **1h,i**), no 1,4-dihydro product was detected (^1H NMR) under the conditions used, even though the most electrophilic and sterically unencumbered 6-position, on the nicotinamide nucleus, was readily available for hydride transfer.

Several other observations also demonstrated that the kinetic product was the 1,4-dihydro derivative, namely, the use of the DCO_2Na as the hydride source provided deuterium in the 4-position exclusively and the fact that very minor isomerization of the 1,4- to its 1,6-isomer occurred, via a separate complex **2** catalyzed rearrangement. Moreover, the total ^1H NMR and UV−vis kinetic analysis clearly supported the fact that NAD^+ model **1a** and catalyst, $[Cp^*Rh(bpy)(H)]^+$, were necessary in the transition state for the 1,4-dihydro product to form, while a distinction was duly noted between reactions in 1:1 H_2O/THF and pure H_2O in that the effect of the substrate concentration on rate was critical with **1a** (Figure 2) but not affected by **3** or NAD^+, respectively. Thus, the formation of a $[Cp^*Rh(bpy)(\mathbf{4a})]^{2+}$ complex, from concerted binding of **1a** with the hydride transfer step, was clearly apparent from the ^1H NMR and UV−vis kinetic results (Table 3 and Supporting Information), but we could not verify this binding via independent ^1H NMR experiments with **2** and **4a**. We further stipulate that a similar concerted binding/hydride transfer step of **3** and NAD^+ to the Cp*Rh metal ion center is also essential for 1,4-dihydro product formation. Therefore, the following equations and equilibria could be established for our mechanistic interpretations of the observed regioselective reductions using NAD^+ (**1a** or **3** would also be treated similarly) as the substrate, eqs 10−13:

$$\underset{\mathbf{2}}{[Cp^*Rh(bpy)(H_2O)]^{2+}} + HCO_2^- \underset{k_2}{\overset{k_1}{\rightleftharpoons}} \underset{\mathbf{A}}{[Cp^*Rh(bpy)(O_2CH)]^+} + H_2O \quad (10)$$

$$\underset{\mathbf{A}}{[Cp^*Rh(bpy)(O_2CH)]^+} \xrightarrow{k_3} \underset{\mathbf{B}}{[Cp^*Rh(bpy)H]^+} + CO_2 \quad (11)$$

$$\underset{\mathbf{B}}{[Cp^*Rh(bpy)H]^+} + NAD^+ \underset{k_5}{\overset{k_4}{\rightleftharpoons}} \underset{\mathbf{C}}{[Cp^*Rh(bpy)(\eta^1\text{-}O\text{-}1,4\text{-NADH})]^{2+}} \quad (12)$$

$$\underset{\mathbf{C}}{[Cp^*Rh(bpy)(\eta^1\text{-}O\text{-}1,4\text{-NADH})]^{2+}} + H_2O \xrightarrow{k_6} \mathbf{2} + 1,4\text{-NADH} \quad (13)$$

Since the concentration of the intermediate **A** was not zero, but with very little change with time, and that of intermediates **B** and **C** never in appreciable quantities, it was appropriate to apply the steady-state approximation to all of them. Furthermore, in good agreement with Steckhan's results, a Michaelis−Menten kinetic phenomenon, indicative of a preequilibrium, was observed experimentally (eq 10).[2b]

Consequently, the steady-state rate equations for intermediates **A**−**C** will be

$$[\mathbf{A}]_{ss} = \frac{[\mathbf{2}][HCO_2^-]}{K_m} \quad (14)$$

$$[\mathbf{B}]_{ss} = \frac{k_3(k_5 + k_6')[\mathbf{2}][HCO_2^-]}{k_4 k_6' K_m[NAD^+]} \quad (15)$$

$$[\mathbf{C}]_{ss} = \frac{k_3[\mathbf{2}][HCO_2^-]}{k_6' K_m} \quad (16)$$

where $k_2' = k_2[H_2O]$, $K_m = (k_2' + k_3)/k_1$, and $k_6' = k_6[H_2O]$.

Therefore, the rate-law equation for the formation of 1,4-NADH becomes

$$\frac{d[1,4\text{-NADH}]}{dt} = \frac{k_3[\mathbf{2}][HCO_2^-]}{K_m} \quad (17)$$

Since complex **2** was a precatalyst rather than a reactant, it was necessary to express [**2**] in eq 17 in terms of the total precatalyst concentration, i.e., $[\mathbf{2}]_0$. Accordingly, application of the steady-state rate equations and mass balance, $[\mathbf{2}]_0 = [\mathbf{2}] + [\mathbf{A}]_{ss} +$

$[\mathbf{B}]_{ss} + [\mathbf{C}]_{ss}$, leads to the following rate-law expression:

$$\frac{d[1,4\text{-NADH}]}{dt} = \{k_3k_4k_6'[\mathbf{2}]_0[HCO_2^-][NAD^+]\}/ \{k_3(k_5 + k_6')[HCO_2^-] + k_4k_6'K_m[NAD^+] + k_4(k_3 + k_6')[HCO_2^-][NAD^+]\} \quad (18)$$

Moreover, since k_6, as $k_6' = k_6[H_2O]$, would be much greater than k_3 and k_5, then eq 18 can be further simplified to the following:

$$\frac{d[1,4\text{-NADH}]}{dt} = \frac{k_3k_4[\mathbf{2}]_0[HCO_2^-][NAD^+]}{k_3[HCO_2^-] + k_4K_m[NAD^+] + k_4[HCO_2^-][NAD^+]} \quad (19)$$

This simplified rate-law expression (eq 19) was still very complicated and contains three terms in the denominator. To obtain a viable final rate-law equation, the concept of a rate-determining step involved in the mechanism was pursued. Thus, two possibilities are proposed for the putative rate-determining step: (1) the formation of the $[Cp^*Rh(bpy)H]^+$, intermediate **B** in eq 11; (2) the formation of intermediate **C** in eq 12. Note that the binding and hydride transfer steps are shown to be concerted. If the formation of $[Cp^*Rh(bpy)H]^+$ is the rate-determining step, which suggests $k_3 \ll k_4$, the first term in the denominator in eq 19 can be neglected, and the above equation would become the following:

$$\frac{d[1,4\text{-NADH}]}{dt} = \frac{k_3[\mathbf{2}]_0[HCO_2^-]}{K_m + [HCO_2^-]} \quad (20)$$

This was also in agreement with the experimental rate orders (ln, ln plots, Supporting Information) found in aqueous media for **3** and NAD^+: [**2**], 1.0; $[HCO_2^-]$, 0.7; [**3** and NAD^+], 0.0, respectively. As a result, the initial rate of formation of **6** or 1,4-NADH is independent of the substrate concentration under these aqueous reaction conditions. Furthermore, the appearance of $[HCO_2^-]$ in the denominator of eq 20 could be the reason for its less than 1 order result (0.7).

In contrast to the kinetic results obtained in water, a profound solvent effect was observed in the presence of a coordinating solvent, THF; when the reactions were conducted in 1:1 H_2O/THF, rather than in aqueous media, the experimental rate law was shown to be dependent on the substrate concentration (experimental order, 1.1). Therefore, the dramatic difference between the obtained experimental rate law expressions for **1a** in 1:1 H_2O/THF and **3** and NAD^+ in water strongly indicated the possibility of a different rate-determining step being involved in the presence of a coordinating solvent. Thus, if the rate-determining step was the formation of intermediate **C** (eq 12), which requires the coordination of the substrate to the Cp*Rh metal ion center followed by hydride transfer to C4, then $k_4 \ll k_3$ and eq 19 could be revised, after neglecting the second term of the denominator:

$$\frac{d[1,4\text{-NADH}]}{dt} = \frac{k_3k_4[\mathbf{2}]_0[NAD^+]}{k_3 + k_4[NAD^+]} \quad (21)$$

However, the disappearance of $[HCO_2^-]$ from the deduced rate-law expression (eq 21) does not accommodate the observed experimental rate order in HCO_2^- ion (order, 0.7; 1:1 H_2O/THF). Considering the above-stated inconsistency that arises during this simplification process, and taking into account the large excess of **3** and NAD^+, the rate constants involved were further fine-tuned to reconcile the observed and derived rate laws. We suggest that the differences between rate constants k_3 and k_4 should be small (i.e., $k_4 \leq k_3$ but not $k_4 \ll k_3$), so that the second term in the denominator in eq 19 cannot be ignored. Consequently, for the reactions conducted in 1:1 H_2O/THF, the rate law depends not only on the precatalyst concentration but also the substrate and the formate ion concentrations, as shown in eq 19. This small adjustment of the rate constants, k_3 and k_4, will bring agreement with the observed rate orders for **1a**: [**2**], 1.0; $[HCO_2^-]$, 0.7; [**1a**], 1.0, in 1:1 H_2O/THF.

The change of the rate-determining step in the mechanism could be attributed to the presence of the coordinating solvent THF, which competitively inhibits the complexation of the substrate with the Cp*Rh metal ion center, causing a significant diminishment of k_4; therefore, a different rate-determining step results. Furthermore, the presence of THF could also reduce the magnitude of k_1 (eq 10), because of its stronger σ-donating ability compared to H_2O, and a greater K_m ($=[k_2' + k_3]/k_1$, where $k_2' = k_2[THF]$) would result, accordingly. The increase in the theoretical K_m, in the presence of THF, would also cause the second term of the denominator in eq 19 to be larger and make it difficult to be ignored in the rate-law expression.

Meanwhile, in attempts to confirm the influence of THF, we also performed the reduction of **1a** in 4:1 H_2O/THF to find the effect of [**1a**] on the initial rate (r_1, Supporting Information) and were gratified to see the reaction order for **1a** decreased to 0.5. Therefore, this finding is conceptually consistent with our proposed interpretation; namely, the rate order in substrate can be drastically reduced by decreasing the THF concentration in the reaction media and, thus, be completely eliminated in the rate law when water was used as the reaction solvent. As a result, eq 20 gives the rate-law expression for reactions occurring in aqueous media, while eq 19 is the rate law for the reactions conducted in 1:1 H_2O/THF.

It can be seen that the reaction rate (v), illustrated in eq 20, would approach a maximum value (v_{max}) at high concentrations of formate ion: $v_{max} = k_3[\mathbf{2}]_0$. Therefore, taking the double reciprocal of eq 20 will give

$$\frac{[\mathbf{2}]_0}{v} = \frac{1}{k_3} + \frac{K_m}{k_3[HCO_2^-]} \quad (22)$$

and a plot of $1/v$ vs $1/[HCO_2^-]$, at a given $[\mathbf{2}]_0$ concentration, is a straight line (Figure 3), which provides the values of k_3 and K_m for the reactions conducted in water (Table 5), and will also allow v_{max} to be calculated.

In good agreement with eq 19 and eq 21, the reaction rate in 1:1 H_2O/THF was found to be independent of formate ion when its concentration was high; therefore, the rate law for the reduction of **1a** should follow the expression shown in eq 21 at high concentrations of formate ion. Thus, in analogy to eq 20, where the reaction rate was found to be independent of the **3** or NAD^+ concentration, taking the double-reciprocal of eq 21 will give eq 23:

$$\frac{[\mathbf{2}]_0}{v} = \frac{1}{k_3} + \frac{1}{k_4[NAD^+]} \quad (23)$$

Therefore, by replacement of $[NAD^+]$ in eq 23 with [**1a**], a plot of $1/v$ vs $1/[\mathbf{1a}]$ at a given $[\mathbf{2}]_0$ concentration (Figure 4) provides k_3 and k_4 for the reactions performed in 1:1 H_2O/THF (Table 5).

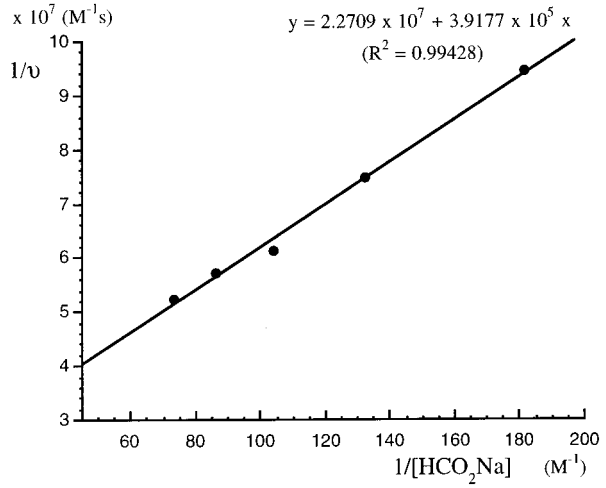

Figure 3. Double-reciprocal plot for the reduction of **3** in water. $[\mathbf{2}]_o = 1.05 \times 10^{-5}$ M.

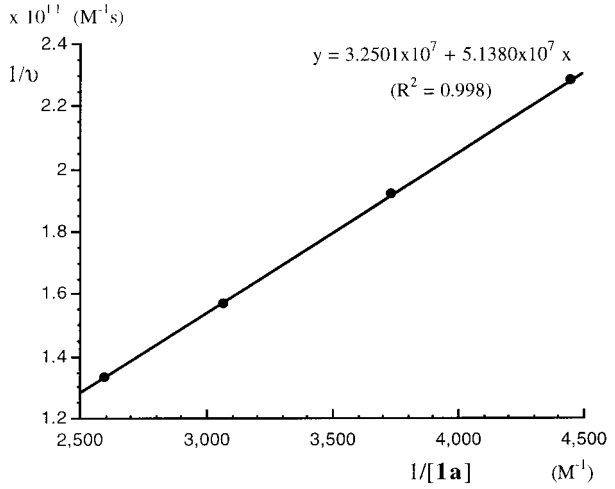

Figure 4. Plot of $1/v$ vs $1/[\mathbf{1a}]$ for rate constants k_3 and k_4, in 1:1 H_2O/THF. $[\mathbf{2}]_o = 2.72 \times 10^{-5}$ M.

Table 5. Pertinent Rate Constants for the Regioselective Reductions of **1a** and **3**

substrate	
1a (1:1 H_2O−THF)	**3** (H_2O)
$k_3 = 1.13 \times 10^{-3}$ (s^{-1})	$k_3 = 4.19 \times 10^{-3}$ (s^{-1})
$k_4 = 7.16 \times 10^{-4}$ (M^{-1} s^{-1})	$K_m = 1.73 \times 10^{-2}$ (M)

Moreover, the observed rate order in substrate **1a** and the obtained rate constants of k_3 and k_4, conducted in 1:1 H_2O/THF at high concentrations of formate ion, plausibly demonstrates that the coordination between the substrates and the Cp*Rh metal ion center is our preferred interpretation of the above-mentioned results and that this coordination step, in concert with hydride transfer, with a rate constant of k_4, becomes the rate-determining step in the presence of THF. To reiterate, we also surmise that although the proposed rate-determining step in water is $[Cp^*Rh(bpy)H]^+$ formation, binding of **3** and NAD^+ to the Cp*Rh metal ion center, in concert with hydride transfer, is also critical for 1,4-dihydro product formation.

The reversibility described in eq 12 was substantiated by the observation of deuteration of H4 in both the pyridinium salt, **1a**, and its 1,4-dihydro derivative, **4a**, in 1:1 D_2O/THF (^1H NMR spectrum) after a prolonged reaction time of >24 h; we also established that this is a general reaction for substrates **1b,d**−**g** and **3** (D_2O). The postulated route to these observed products

Scheme 1. Plausible Deuterium Exchange/Deuteride Reduction Mechanism for NAD^+ Models, **1a,b,d**−**g** and **3**, and NAD^+ Itself in the Presence of D_2O with Ligand bpy Removed from the Cp*Rh Structure for Simplicity

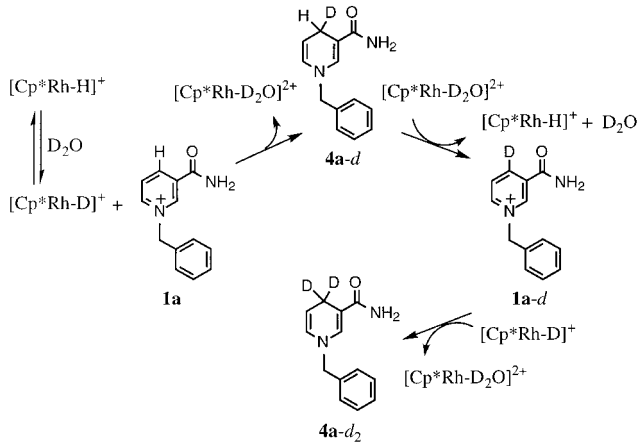

can emanate from deuterium exchange of the $[Cp^*Rh(bpy)H]^+$ with D_2O to provide $[Cp^*Rh(bpy)D]^+$, which could transfer its deuteride to **1a** and lead to the 1,4-product, **4a**-*d*, containing one deuterium at the C4 position. The subsequent catalyzed oxidation of **4a**-*d* should then remove H4 rather than D4 to give the $[Cp^*Rh(bpy)H]^+$, due to a potential H/D kinetic isotope effect, and **1a**-*d* would result. The formed **1a**-*d* could further accept a deuteride from the $[Cp^*Rh(bpy)D]^+$ complex to yield **4a**-d_2, which bears two deuterium at C4 (Scheme 1).

Therefore, our above-mentioned kinetic analysis, deuterium exchange results, and the data in Table 3 allow us to propose a plausible catalytic cycle for the regioselective reduction of the NAD^+ models, **1a** or **3**, and NAD^+ itself, with **2** as the precatalyst and sodium formate as the hydride source (Scheme 2). The reaction of **2** with HCO_2Na provides the $[Cp^*Rh(bpy)(OC(O)H)]^+$ complex, **A**, which decomposes to the hydride complex, $[Cp^*Rh(bpy)(H)]^+$, **B**, via a β-hydrogen elimination reaction to produce CO_2.[2b,5a] The critical role of the amide functionality is to coordinate to the Cp*Rh metal center, along with concerted hydride transfer, includes a kinetically favorable six-membered ring transition state (**C, I** or **I′** are thought to be viable possibilities for this process; ring-slip, $\eta^5-\eta^3$, in concert with binding and hydride transfer[6] or concerted binding with hydride transfer, which fit the kinetic and relative rate data), which further provides a driving force for regioselective hydride transfer at C4 to provide intermediate **C**, **II**. It should also be noted that hydride transfer, **I** or **I′** to **II** in **C**, could be a reversible process as suggested by the above-stated deuterium exchange experiments (Scheme 1). Finally, displacement of the 1,4-dihydro product and recycling **2**, via a H_2O molecule, completes the catalytic cycle.

Furthermore, during the coordination process of the 3-substituent to the Cp*Rh metal center, the induced electronic effect of the bound carbonyl group may also cause the C4 position to be a more electrophilic site toward hydride transfer, while the very prominent electron-withdrawing effect of the 1-substituent (i.e. benzyl in **1a**; ribose in **3** or NAD^+) is also critical for effective rates of hydride transfer. Moreover, we suggest that the other 3-substituted pyridinium NAD^+ models (**1b,d**−**g**), which can coordinate to the Cp*Rh metal center and exert an electron-withdrawing effect at C4, would undergo a similar mechanism depicted in Scheme 2.

Our results also demonstrate no apparent role of the pyrophosphate and adenosine constituents in the reductive reactions,

Scheme 2. Plausible Catalytic Cycle for the Regioselective Reduction of NAD^+ and Models, **1a,b,d−g**, and **3**

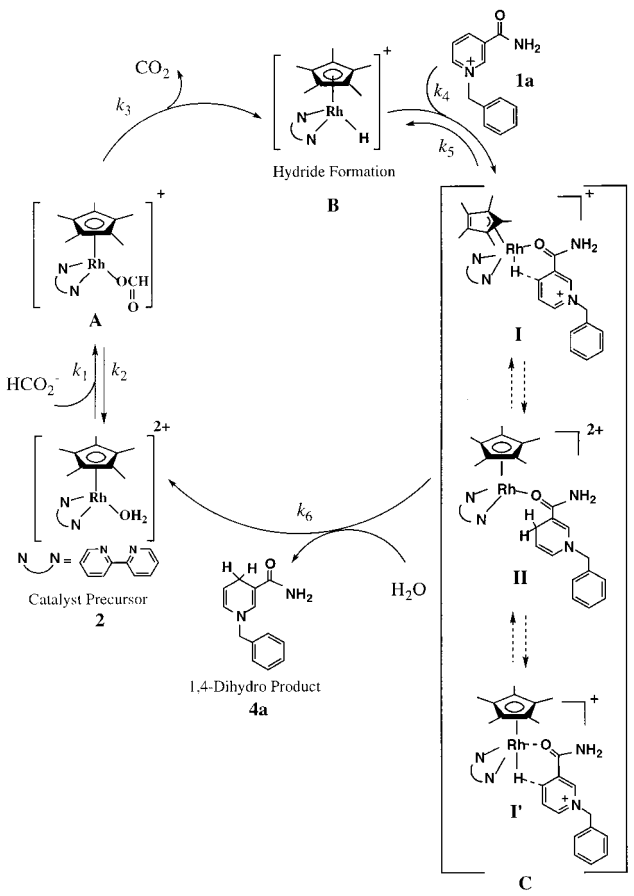

and more importantly, the role of the amide carbonyl or other coordinating groups at the 3-position may also be prevalent in other reported 1,4-regioselective reduction of NAD^+ models by transition metal hydrides.[2c,f−h,4a] It is also worthwhile to mention that, in contrast to our findings, a sterically hindered porphyrin Ru−H regeoselectively provided the 1,6-isomer as the sole kinetic product with substrate **1c**[2d] and that the noncoordinating, direct hydride reducing agent, $NaBH_4$, only provides a mixture of 1,2- and 1,6-dihydro isomers in the cases of **1f,g**, with no 1,4-isomer isolated,[11] in which the boron hydride appears to attack the most electrophilic carbons of C2 and C6 on the pyridinium ring. Both these latter results further strengthen our mechanistic conclusions on the regioselective reduction reactions of NAD^+ and the models presented in this paper (Scheme 2).

Conclusions

The critical result in the regioselective reduction of the NAD^+ models, **1a** and **3**, and NAD^+ itself with $[Cp^*Rh(bpy)H]^+$, to exclusively form the kinetic 1,4-dihyro analogue, for possible applications in cofactor regeneration, coupled to biocatalytic reactions that convert achiral compounds to chiral compounds,[3,4] was the binding of the NAD^+ models, and NAD^+ itself, to Cp*Rh metal ion center, and thus, we consider this step, in concert with hydride transfer to C4, crucial for 1,4-dihydro product formation, regardless of the solvent system. As can be observed in Table 3, any substituent in the 3-position that can potentially bind to the Cp*Rh metal ion center forms the corresponding 1,4-dihydro derivative (eqs 4 and 6). The binding step also causes electron-withdrawing effects of the bound substituent and a similar, but more dominant effect, of the 1-substituent to facilitate hydride transfer to C4. The relative rates with the better σ-donation substituents appear to be slightly higher, but small differences were noted and apparently the critical factor was binding of the substrate to the Cp*Rh metal ion center that causes hydride transfer to occur to provide the corresponding 1,4-dihydro derivative.

What was also apparent from our extensive kinetic and mechanistic results was that NAD^+ model **3** with a 1-ribose methyl phosphate group (H_2O, pH 6.5) was reduced by the catalyst, $[Cp^*Rh(bpy)H]^+$, at initial rates that were comparable to NAD^+ itself, while **3** and NAD^+ had comparable TOF values, via NMR and UV−vis analysis, that were ∼3−4 times those for **1a** (1:1 H_2O/THF). Furthermore, the substituents directly bonded to the nitrogen of the nicotinamide nucleus also greatly affect the rate of regioselective reduction, while the pyrophosphate and adenosine groups of NAD^+ do not apparently have any significant electronic/steric effect on the rate of hydride transfer to C4.

Finally, we wish to categorize $[Cp^*Rh(bpy)H]^+$ as an example of a biomimetic enzyme hydride that clearly can bind to the substrate functional group and, in that process, constricts the transition state for exclusive hydride transfer to a specific carbon atom in proximity to the binding site. Future papers on the regioselective reduction will also describe the results of the generation of $[Cp^*Rh(bpy)H]^+$ via electrochemical pathways to provide cofactor regeneration with the model NAD^+ compounds, including organic solvent effects, and the use of both $[Cp^*Rh(bpy)H]^+$ and the NAD^+ models in conjunction with enzymes for chiral organic synthesis.[15]

Experimental Section

Instrumentation. Unless otherwise specified, NMR spectra were recorded on a Bruker AMX-300, AMX-400, or DRX-500 MHz spectrometer at room temperature. The ^1H NMR chemical shifts are reported in ppm downfield from 3-(trimethylsilyl)propionate-2,2,3,3-d_4 (sodium salt) and referenced to residual solvent resonances (^1H NMR: 4.67 for D_2O), where the signals are given followed by multiplicity, coupling constants J in Hertz, and integration in parentheses. For complicated coupling patterns, e.g. δ (dt, $J = 3.2, 7.6$, 1H), the first doublet (d) represents the smaller coupling and the second triplet (t) indicates the larger coupling. Assignments are provided for key moieties only. The $^{31}P\{^1H\}$ NMR chemical shifts were referenced to 85% H_3PO_4(aq) as an external standard.

UV−vis spectra were measured with a Hewlett-Packard instrument, model 8452A diode-array UV−vis spectrophotometer. IR spectra were obtained on a Nicolet instrument, model Impact 400 FT-IR spectrophotometer. Unless otherwise specified, IR samples were prepared in solid (KBr pellets) and absorptions are reported in wavenumbers (cm^{-1}). Electrospray/MS and FAB/MS spectra were acquired on a VG Quattro spectrometer and VG 70 spectrometer, respectively. The pH values were obtained with an Orion 601A pH meter equipped with an Orion semimicro combination pH electrode, and those in D_2O were converted to pD (pH + 0.4 = pD). Elemental analyses were performed at the Department of Chemistry, University of California, Berkeley, CA.

(11) (a) Büchi, G.; Coffen, D. L.; Kocsis, K.; Sonnet, P. E.; Ziegler, F. E. *J. Am. Chem. Soc.* **1966**, *88*, 3099 and references therein. (b) Schmidt, R. R.; Berger, G. *Chem. Ber.* **1976**, *109*, 2936.

(12) Eisen, M. S.; Haskel, A.; Chen, H.; Olmstead, M. M.; Smith, D. P.; Maestre, M. F.;Fish, R. H. *Organometallics* **1995**, *14*, 2806.

(13) Sheldrick, G. M. *SHELXTL*, v. 5; 1994. Tables of neutral atom scattering factors, f' and f'', and absorption coefficients are from: *International Tables for Crystallography*; Wilson, A. J. C., Ed.; Kluwer Academic Publishers: Dordrecht, The Netherlands, 1992; Vol. C, Tables 6.1.1.3 (pp 500−502), 4.2.6.8 (pp 219−222), and 4.2.4.2 (pp193−199), respectively.

(14) Parkin, S. R.; Moezzi, B.; Hope, H. *J. Appl. Crystallogr.* **1995**, *28*, 53.

(15) Lo, H. C.; Fish, R. H. *Angew. Chem.*, in press.

J. Young NMR tubes, featuring a resealable Teflon threaded cap, were presilylated with 1,1,1,3,3,3-hexamethyldisilazane to avoid acid-catalyzed aquaphilic reactions. Unless otherwise noted, all reactions and manipulations were conducted under a nitrogen atmosphere in a Vacuum Atmospheres glovebox or by using Schlenk techniques.

Materials. $[Cp^*RhCl_2]_2$ was purchased from Colonial Metals and was used as received. $[Cp^*Rh(H_2O)_3]OTf_2$ was prepared according to the literature method.[12] The deuterated solvents (D_2O and THF-d_8) were purchased from Cambridge Isotope Laboratories and were degassed by bubbling argon through commercially supplied containers and stored under nitrogen for general use. β-Nicotinamide adenine dinucleotide (NAD^+, sodium salt), β-1,4-NADH (disodium salt), β-nicotinamide mononucleotide, and reduced form of β-nicotinamide mononucleotide (disodium salt) were purchased from Sigma and were used without further purification. Water (HPLC grade) was purchased from Aldrich. Pyridine (over calcium hydride), 3-picoline (over calcium hydride), ethyl ether (over sodium benzophenone ketyl), THF (over sodium benzophenone ketyl), and methylene chloride (over calcium hydride) were refluxed with proper drying agents in parentheses and distilled under nitrogen. Methanol (used for the syntheses of **3** and **6**) was dried by treatment with Mg metal using the procedure given for superdry ethanol. Benzyl chloride and benzyl bromide was distilled, and all other solvents used were deoxygenated with argon or nitrogen prior to use. $[(CH_3)_4N]OTf$ was used as an internal standard in the NMR tube reactions.

General Procedure for the Synthesis of NAD^+ Models, 1. Unless otherwise stated, the chloride or bromide salts of NAD^+-model substrates were prepared according to related published methods;[7] however, THF was used as the reaction solvent so as to simplify the purification process (yields, 41−99%). Anion exchange was conducted either by utilizing AgOTf (1.0 equiv, in MeOH) or NaOTf (1.05 equiv, in acetone). After solvent removal of the filtrate, the crude product was further purified by recrystallization from (acetone−CH_2Cl_2 = 1)−Et_2O, followed by refrigeration at −15 °C. The crystals were collected on a glass-fritted funnel and washed with acetone−Et_2O (ratio = 1:4, 0 °C) and were dried in vacuo over P_2O_5 in 86−97% yield. The procedure for the preparation of **1d** is shown as an example, while all the spectroscopic and analytical data for **1a**−**c**,**e**−**i** and **5** were placed in the Supporting Information.

1-Benzylthionicotinamide, Triflate Salt, 1d. A 100 mL two-necked Schlenk flask fitted with a Claisen head was equipped with a condenser and an addition funnel. The reaction unit was flame dried under vacuum and cooled to room temperature under nitrogen. Under positive N_2 pressure, thionicotinamide (98%, 2.82 g, 20 mmol) was added, followed by the addition of THF (40 mL) via syringe. The resulting suspension was then heated under gentle reflux to give a clear yellow solution. Benzyl chloride (2.53 g, 20 mmol) in 20 mL of THF was then placed in the addition funnel and added to the reaction flask dropwise over a period of 4 h under nitrogen with reflux. A yellow precipitate was observable when the addition was complete. The reaction mixture was allowed to reflux for another 4 h under nitrogen, after which time the reaction flask was cooled in an ice-bath and the reaction mixture was further concentrated to two-thirds of the original volume on a high-vacuum line. The precipitate was then collected on a glass-fritted funnel and washed with acetone until there was not an appreciable smell of thiols (done in a well-ventilated hood). The collected yellow powder was further purified by three fractional recrystallizations from MeOH−Et_2O at −15 °C. The resulting crystals were washed with acetone dried in vacuo over P_2O_5 to give the corresponding chloride salt (1.69 g) in 32% yield. Anion exchange was achieved by using NaOTf (1.05 equiv, in acetone). The crude product was further purified by two fractional recrystallizations from MeOH−Et_2O at −15 °C, and the collected crystals were washed with acetone−Et_2O (ratio = 1:4, 0 °C) to give the title compound as yellow crystals in 84% yield. ^1H NMR (D_2O): δ 9.31 (s, 1H, H2 on Py), 8.88 (d, J = 6.4, 1H, H6 on Py), 8.71 (d, J = 8.4, 1H), 8.00 (dd, J = 6.0, 8.1, 1H), 7.41 (app s, 5H), 5.77 (s, 2H, $-CH_2Ph$). Anal. Calcd for $C_{14}H_{13}F_3N_2O_3S_2$ (378.43): C, 44.43; H, 3.47; N, 7.40. Found: C, 44.36; H, 3.56; N, 7.65.

Tetramethylammonium Triflate. This salt was used as an internal standard in the NMR tube reactions. The title compound was prepared by reaction of $[(CH_3)_4N]Cl$ with AgOTf (1.0 equiv) in methanol and was purified by recrystallization from hot MeOH−Et_2O, followed by refrigeration at −15 °C. The white crystals were collected on a glass-fritted funnel, washed with MeOH−Et_2O (ratio = 1:4, 0 °C), and dried in vacuo over P_2O_5 (yield, 79%). ^1H NMR (D_2O): δ 3.08 (s). Anal. Calcd for $C_5H_{12}F_3NO_3S$ (223.25): C, 26.90; H, 5.43; N, 6.28. Found: C, 26.88; H, 5.68; N, 6.54.

[Cp*Rh(η^2-(*N*,*N*)-2,2′-bipyridyl)(H_2O)]OTf_2, 2. A 50 mL Schlenk flask equipped with a stirbar was charged with $[Cp^*Rh(H_2O)_3]OTf_2$ (200 mg, 339 × 10^{-3} mmol) and 2,2′-bipyridyl (53 mg, 340 × 10^{-3} mmol) and was capped with a septum. Standard Schlenk techniques were then performed to deoxygenate the solid mixture, and H_2O (4 mL, deoxygenated) was added via syringe through septum under nitrogen to give a suspension. The reaction mixture was allowed to stir at room temperature under nitrogen; in general, the reaction was complete within 4 h as determined by the disappearance of the bipyridyl ligand and the presence of a clear yellow-orange solution. Any insoluble species were filtered off with a glass-fritted funnel through a 1-in. Celite bed via cannula. The filter cake was washed with a small amount of H_2O (deoxygenated) until the filter cake was colorless, and the solvent of the filtrate was removed on a high-vacuum line to give a yellow powder. The resulting powder was further purified by recrystallization from hot H_2O under nitrogen, followed by refrigeration at 5 °C. The crystals were collected and washed with CH_2Cl_2−Et_2O (ratio = 1, 0 °C) and dried in vacuo over NaOH to give **2** (185 mg, 77%) as a yellow-orange solid. The title complex was found to be stable as a solid in the air. ^1H NMR (D_2O): δ 9.04 (d, J = 4.6, 2H, H^6 on Py), 8.39 (d, J = 7.3, 2H), 8.24 (t, J = 7.4, 2H), 7.83 (app t, J = 6.6, 2H), 1.61 (s, 15H). IR: 3085, 2914, 1604 (cm^{-1}). Anal. Calcd for $C_{22}H_{25}F_6N_2O_7RhS_2 \cdot H_2O$ (728.56): C, 36.27; H, 3.74; N, 3.85. Found: C, 36.30; H, 3.62; N, 4.14. Suitable single crystals for X-ray diffraction analysis were obtained by recrystallization from MeOH−Et_2O at −15 °C.

***β*-Nicotinamide Ribose-5′-methyl Phosphate, 3.** β-Nicotinamide mononucleotide (503 mg, 1.44 mmol), *p*-(dimethylamino)pyridine (DMAP) (17.6 mg, 1.44 × 10^{-1} mmol), and a stirbar were placed in a 250 mL flame-dried Schlenk flask. Standard Schlenk techniques were performed to deoxygenate the solid mixture, and methanol (125 mL, dried) was then added via cannula to dissolve the solids under nitrogen. Under positive N_2 pressure, 1,3-dicyclohexylcarbodiimide (DCC) (635 mg, 3.08 mmol) was added in one portion to the reaction mixture, and the resulting solution was stirred at room temperature. The reaction progress was followed by TLC (SiO_2, MeOH−CH_2Cl_2 = 3, R_f = ∼0.3). After 3 h, additional 1,3-dicyclohexylcarbodiimide (656 mg, 3.18 mmol) was added, and the reaction mixture was allowed to stir for another 24−30 h. The white precipitate was filtered out on a glass-fritted funnel and washed with CH_2Cl_2 (5 mL × 2). The collected filtrate was concentrated on a high-vacuum line to give an oily residue. The mixture was then taken up with H_2O (∼1.5 mL, deoxygenated), and any insoluble species were further filtered off and rinsed with CH_2Cl_2 (2 mL). The solvent of the filtrate was stripped, and a small amount of eluting solvent was used to dissolve the obtained residue. The mixture was then purified by column chromatography (column diameter, 20 mm; column height, 40 cm) with SiO_2 (CH_3OH−CH_2Cl_2 = 3, deoxygenated) under nitrogen. The eluant was dried on a high-vacuum line to give a gummy residue, which can be solidified by addition of a small amount of CH_2Cl_2, followed by removal of the solvent on a high vacuum line, to yield the title compound dried in vacuo over P_2O_5 as a white solid (261 mg, 52%), or can be solidified upon sitting at −15 °C. The title compound appears to be light-sensitive and somewhat air-sensitive, and thus, storing at low temperature under subdued room light is highly recommended. ^1H NMR (D_2O): δ 9.35 (s, 1H, H^2 on Py), 9.16 (d, J = 6.3, 1H, H^6 on Py), 8.87 (d, J = 8.1, 1H), 8.19 (dd, J = 6.3, 8.1, 1H), 6.11 (d, J = 5.1, 1H, $H^{1'}$), 4.53 (m, 1H), 4.43 (t, J = 5.1, 1H), 4.33 (dd, J = 2.7, 5.1, 1H), 4.21 (ddd, J = 2.5, 4.4, 12.1, 1H), 4.04 (ddd, J = 2.3, 5.1, 12.1, 1H), 3.46 (d, $^3J_{HP}$ = 10.8, 3H, $-CH_3$). $^{31}P\{^1H\}$ NMR (202.3 MHz, D_2O): δ 0.31. Anal. Calcd for $C_{12}H_{17}N_2O_8P \cdot 0.1H_2O \cdot 0.1CH_3OH$ (353.29): C, 41.13; H, 5.03; N, 7.93. Found: C, 41.14; H, 5.13; N, 7.46.

General Procedure for the Synthesis of 1,4-Dihydropyridine Derivatives, with 4a as an Example. The 1,4-dihydropyridine derivatives were prepared according to the related literature methods.[7] In a

typical reaction, a 25 mL Schlenk flask equipped with a stirbar was charged with the chloride salt of **1a** (28 mg, 111×10^{-3} mmol), Na_2CO_3 (38.7 mg, 365.1×10^{-3} mmol), and $Na_2S_2O_4$ (72 mg, 343×10^{-3} mmol). Schlenk techniques were performed to deoxygenate the solids, and H_2O (3 mL, deoxygenated) was then added to the reaction flask via syringe under nitrogen. The reaction mixture was heated in a 45 °C oil bath for 10 min, after which time yellow oily drops were deposed on the wall of the reaction flask. The reaction flask was then cooled in an ice-bath, and the solvent of the reaction mixture was pipeted off under positive N_2 pressure. The resulting oily residue was washed with H_2O (1 mL × 5, deoxygenated), and the washings were pipeted off under N_2. The residual water of the obtained oil was further removed azeotropically with CH_2Cl_2 (5 mL × 2) on a high-vacuum line to give the corresponding 1,4-dihydropyridine derivative, **4a**, as a pale-yellow solid (yield, 78%). ^{1}H NMR ($CDCl_3$): δ 7.38−7.20 (m, 5H), 7.14 (d, $J = 1.6$, 1H, H^2 on Py), 5.72 (qd, $J = 1.6$, 8.1, 1H, H^6 on Py), 5.35 (br s, 2H, $-NH_2$), 4.73 (td, $J = 3.5$, 8.1, 1H, H^5 on Py), 4.27 (s, 2H, $-CH_2Ph$), 3.15 (dd, $J = 1.6$, 3.5, 2H, H^4 on Py). ^{1}H NMR (D_2O−THF-d_8): δ 7.60−7.45 (m, 5H), 7.35 (s, 1H, H^2 on Py), 6.01 (d, $J = 8.1$, 1H, H^6 on Py), 4.94, (td, $J = 3.6$, 8.1, 1H, H^5 on Py), 4.54 (s, 2H, $-CH_2Ph$), 3.28 (br s, 2H, H^4 on Py). In most cases, the 1,4-dihydropyridine derivatives can be isolated in good purity by the above stated procedure. However, in some cases (**4c**−**e**) fractional precipitation was required in order to obtain pure products.

***β*-1,4-Dihydronicotinamide Ribose-5′-methyl Phosphate, 6.** The 1,4-dihydro form of β-nicotinamide mononucleotide (147 mg, 371×10^{-3} mmol), *p*-(dimethylamino)pyridine (6.1 mg, 50×10^{-3} mmol), pyridinium *p*-toluenesulfonate (53 mg, 211×10^{-3} mmol), and a stirbar were placed in a 100 mL flame-dried Schlenk flask. Schlenk techniques were performed to deoxygenate the solid mixture, and methanol (40 mL, dried) was then added via cannula through septum under nitrogen. Under positive N_2 pressure, 1,3-dicyclohexylcarbodiimide (209 mg, 1013×10^{-3} mmol) was added in one portion to the reaction mixture, and the resulting solution was stirred at room temperature under subdued room light. After 1 h, additional pyridinium *p*-toluenesulfonate (53 mg, 211×10^{-3} mmol) and 1,3-dicyclohexylcarbodiimide (261 mg, 1265×10^{-3} mmol) were added, and the resulting mixture turned slightly cloudy. The reaction mixture was allowed to stir for another 7 h to complete the reaction. TLC analysis of the final reaction mixture was conducted in a nitrogen-filled glovebox (Cellulose TLC: MeOH, $R_f \sim 0.4$, second spot, streaking and highly fluorescent). After the removal of solvent on a high-vacuum line, the residue was taken up with H_2O (2.5 mL) in a glovebox and any insoluble species were filtered off and rinsed with a small amount of CH_2Cl_2 (~2 mL × 2). The solvent of the combined filtrate was stripped, and a small amount of methanol was used to dissolve the obtained residue. The resulting mixture was then purified by column chromatography (column diameter, 20 mm; column height, 35 cm) with Sephadex LH-20 (MeOH, deoxygenated) under nitrogen. The column separation of the mixture was monitored by a UV−vis detector to give the title compound coeluting with sodium *p*-toluenesulfonate. The solvent of the collected eluant was removed on a high vacuum line, and a pale yellow solid was obtained. According to ^{1}H NMR spectroscopy and elemental analysis, the obtained pale yellow solid dried in vacuo over P_2O_5 contains 0.33 mol of **6** ($C_{12}H_{18}O_8N_2PNa$, 372.28) and 0.67 mol of sodium *p*-toluenesulfonate, **6′** ($C_7H_7O_3SNa$, 194.20) with a yield of 75% (222.2 mg, based on nicotinamide). The title compound is both light- and air-sensitive. ^{1}H NMR (D_2O): δ 6.98 (s, 1H, H^2 on Py), 6.04 (d, $J = 8.3$, 1H, H^6 on Py), 4.87 (td, $J = 3.4$, 8.2, 1H, H^5 on Py), 4.77 (d, $J = 6.8$, 1H, $H^{1'}$), 4.16−4.09 (m, 2H), 3.97 (m, 1H), 3.82 (m, 2H, $H^{5'}$), 3.43 (d, $^3J_{HP} = 10.8$, 3H, $-CH_3$), 2.92 (br s, 2H, H^4 on Py). ^{31}P{^{1}H} NMR (161.9 MHz, D_2O): δ 2.38. Anal. Calcd for (0.33**6**·0.67**6′**)·0.4H_2O·0.1 CH_3OH (263.38, approximately): C, 39.90; H, 4.54; N, 3.51; S, 8.16. Found: C, 39.56; H, 4.64; N, 3.57; S, 7.82.

General Procedure for NMR Mechanistic Study on Reduction of NAD^+ Models. In a typical reaction, a J. Young NMR tube was charged with models **1a**−**i** (2.39×10^{-1} mmol), **2** (2.39×10^{-3} mmol), and HCO_2Na (2.63×10^{-1} mmol), and Schlenk techniques were then conducted to deoxygenate the solid mixture. Under positive N_2 pressure, a deuterated solvent (for **1a**−**i**, 1:1 D_2O/THF-d_8; for **3** and NAD^+, D_2O; 0.75 mL, deoxygenated) was added, and the NMR tube was sealed. Right after the addition of solvent, the NMR tube was placed in a liquid-nitrogen bath, and the resulting mixture were further degassed by two successive freeze−pump−thaw cycles. After thawing of the reaction mixture, the contents were immediately frozen in a salted ice bath and covered with aluminum foil. The reaction was then followed by the ^{1}H NMR spectroscopy at 26 °C after a speedy thawing out. The given relative rates and turnover frequencies were determined by the decreasing integration of the corresponding pyridinium salts measured against an internal standard, $[(CH_3)_4N]OTf$, during the first 2 h of reaction. The ratios of 1,4- and 1,6-isomers of **4a,b,d**−**g** were obtained by comparison of the resonance signals with those of authentic samples, where the diagnostic signal is the resonance for $-CH_2Ph$ moiety which can be identified unambiguously in the ^{1}H NMR spectrum of the reaction mixture. Additionally, the signals of H^2 and H^6 protons on the pyridine ring of **6** (or 1,4-NADH) were used for the isomer determination. It was further noticed that the signal for H4 in **1** disappeared after a prolonged reaction time (>24 h), and in addition, the signal associated with the H4 protons of **4** also disappeared after >24 h of reaction time; this was found to be a general phenomena for all NAD models that gave 1,4-dihydro products.

Control Experiments and Experimental Observations for Deuterium Exchange/Deuteride Reductions with 1a and 4a. Similar reaction conditions described in the ^{1}H NMR mechanistic studies were utilized for these deuterium exchange/deuteride reduction experiments. A solution of protio-**1a** or protio-**4a** in 1:1 D_2O/THF-d_8 was followed by ^{1}H NMR spectroscopy for at least 24 h, and no detectable deuterium on the H4 proton(s) was observed, in which the signal integration and shape remained unchanged. Likewise, the reaction of protio-**1a** in the presence of complex **2** (1 mol %) in 1:1 D_2O/THF was analyzed, and again, no deuteration of the pyridinium ring was detected (^{1}H NMR, 24 h). The deuterium exchange/deuteride reduction of the H4 proton-(s) in the reaction of protio-**4a** in the presence of complex **2** (1 mol %) in 1:1 D_2O/THF was observed to occur with a decrease in the signal integration and change of line shape, along with the isomerization to give the 1,6-isomer of **4a** (<5%), under the conditions described, but no detectable amount of the oxidized pyridinium salt could be found in the reaction mixture. However, upon prolonged reaction time (>24 h), a complex ^{1}H NMR spectrum was observed, in which deuteration of the H4 proton(s) for **1a**-*d*, **4a**-*d*, and **4a**-d_2 can be clearly identified by ^{1}H NMR spectroscopy (see the proceeding General NMR section for chemical shift data).

Kinetic and Thermodynamic Data for 1-Benzylnicotinamide Triflate, 1a (1:1 H_2O/THF), *β*-Nicotinamide Ribose-5′-Methyl Phosphate, 3, (H_2O, pH = 6.5), and NAD^+ in the Regioselective Reduction with [Cp*Rh(bpy)(H_2O)]($OTf)_2$, 2, and Formate Ion. The kinetic experiments were carried out on a Hewlett-Packard 8452A diode array UV−vis spectrophotometer, attached to a circulating water bath (VWR 1160). For experiments conducted at different temperatures, the circulating water bath, as well as the UV−vis instrument, were warmed for at least 1 h before the kinetic studies were initiated. A solution of H_2O/THF (similar for 1:1 or 1:4 ratios) was used for all the kinetic experiments, unless otherwise specified. A stock solution of **1a** (0.018 M), **2** (6.23×10^{-3} M), and sodium formate (0.25 M) was made for the kinetic experiments in 1:1 H_2O/THF.

A general procedure for the kinetic experiments is as follows: A solution of 1-benzylnicotinamide triflate, **1a** (4.29×10^{-3} M), and sodium formate (0.0539 M) was made in a volumetric flask (10 mL) under N_2 in a 1:1 H_2O/THF mixture (the different concentrations of **1a** and sodium formate used for the kinetic experiments are reported in the tables in the Supporting Information). A 3.0 mL aliquot of this solution was transferred to a thermostated UV−vis cell by using an air-free syringe, which also was purged with N_2 gas. The sample was then brought to the desired temperature for 30−60 min in the UV−vis spectrophotometer thermostated cell holder. Then, 23 μL of a 6.23×10^{-3} M stock solution of $[Cp^*Rh(bpy)(H_2O)]^{2+}$, **2**, was added via syringe under a positive N_2 pressure and quickly mixed with the solution, and the absorbance increase at 354 nm was immediately recorded. The experiment was carried out for 2 h, and the formation of the product, 1-benzyl-1,4-dihydronicotinamide, **4a**, was followed, with the change in absorbance being recorded every 90 s. Some kinetic experiments were carried out until all the starting material was converted

to product. The induced volume change was taken into account for the calculation of the turnover frequency (TOF) as follows, where A_{354} = absorbance at 354 nm, ϵ = molar absorptivity, d = optical path length, c_{Rh} = catalyst concentration, and t = reaction time, respectively:

$$\mathrm{TOF} = \frac{A_{354}}{\epsilon d c_{\mathrm{Rh}} t} \quad \mathrm{h}^{-1}$$

The kinetic experiments for the β-nicotinamide ribose-5′-methyl phosphate, **3**, and natural NAD^+ were followed by the same general procedure described above. These kinetic experiments were carried out in H_2O, and the concentration of β-nicotinamide-5′-ribose methyl phosphate (**3**) or NAD^+, sodium formate, and $[Cp^*Rh(bpy)(H_2O)]^{2+}$ (**2**) were in the order of 1.50×10^{-3}, 0.0186, and 1.42×10^{-5} M, respectively. λ_{max} for **6** and 1,4-NADH was 336 nm. In all the initial rate plots, time 0 s was removed from the plots of concentration versus time.

Electrochemical Measurements. These were carried out by means of cyclic voltammetry using a standard three-electrode cell with a glassy carbon electrode referred to a Ag/AgCl reference electrode. The solutions were generally water/THF with an appropriate buffer salt. All of the electrochemical responses of the compounds **1a**−**i** exhibited a chemically irreversible peak in voltammetric experiments using 20−50 mV/s sweep rates.

X-ray Data Collection, Solution, and Refinement. Data for the crystal structure determination were collected on a Siemens R3m/v diffractometer at 130(2) K with the use of Mo Kα radiation. The structure was solved by direct methods. Refinement was carried out with the SHELXTL 5 package.[13] Hydrogens were included at idealized positions and refined using a riding model except for those on water, which were located in a difference Fourier map and fixed. There is disorder at the site of the coordinated water, which is modeled as 0.70 water and 0.30 methanol. In addition, there is a water of solvation that is only present when the coordinated water, and not methanol, is present. All non-hydrogen atoms except these were refined with anisotropic thermal parameters. An absorption correction (XABS2)[14] was applied. The largest feature in the final difference map had a peak value of 0.62 e $Å^{-3}$, 0.96 Å from F5 of a triflate group. All other features were less than 0.54 e $Å^{-3}$.

Acknowledgment. We gratefully acknowledge Department of Energy funding from the Advanced Energy Projects and Technology Research Division, Office of Computational and Technology Research, under Contract No. DE AC03-76SF00098. We especially appreciate and acknowledge Dr. Roberto A. Sánchez-Delgado, IVIC, Caracas, Venezuela, for the critical analysis of our manuscript.

Supporting Information Available: Analytical data, kinetic data, ln r_i vs ln concentration plots, tables, and activation parameters for the reduction of **1a**, **3**, and NAD^+ with in situ generated $[Cp^*Rh(bpy)H]^+$, spectroscopic and analytical data for **1a**−**c**,**e**−**i**, and **5**, X-ray crystallographic files, in CIF format, for the structure of **2**, and a detailed listing of crystallographic data collected parameters (PDF). This material is available free of charge via the Internet at http://pubs.acs.org.

IC010562Z